ISSN 0030-400X, Optics and Spectroscopy, 2016, Vol. 121, No. 6, pp. 790–797. © Pleiades Publishing, Ltd., 2016.
Original Russian Text © A. Sargsyan, A. Amiryan, T.A. Vartanyan, D. Sarkisyan, 2016, published in Optika i Spektroskopiya, 2016, Vol. 121, No. 6, pp. 848–856.

SPECTROSCOPY OF ATOMS AND MOLECULES

Studying the Regime of Complete Decoupling of the Bond between the Electron and Nuclear Moments at the D_1-Line of the ^{39}K Potassium Isotope Using a Spectroscopic Microcell

A. Sargsyan[a], A. Amiryan[a, b], T. A. Vartanyan[c, *], and D. Sarkisyan[a]

[a] *Institute for Physical Research, National Academy of Sciences of Armenia, Ashtarak-2, 0203 Armenia*

[b] *Laboratoire Interdisciplinaire Carnot de Bourgogne, UMR CNRS 6303, Université Bourgogne–Franche-Comté, Dijon, France*

[c] *St. Petersburg State University of Information Technologies, Mechanics, and Optics, St. Petersburg, 197101 Russia*

**e-mail: tigran@vartanyan.com*

Received July 21, 2016

Abstract—Atomic transitions of the ^{39}K potassium isotope in strong (up to 1 kG) longitudinal and transverse magnetic fields have been studied with a high spectral resolution. It has been shown that crossover resonances are almost absent in the saturated absorption spectrum of potassium vapors in a 30-μm-thick microcell. This, together with the small spectral width of atomic transitions (~30 MHz), allows one to use the saturated absorption spectrum for determining frequencies and probabilities of individual transitions. Among the alkali metals, potassium atoms have the smallest magnitude of the hyperfine splitting of the lower level. This allows one to observe the break of the coupling between the electronic and nuclear angular momentums at comparatively low magnetic fields $B > 500$ G, i.e., to implement the hyperfine Paschen–Back regime (HPB). In the HPB regime, four equidistantly positioned transitions with the same amplitude are detected in circularly polarized light (σ^+). In linearly polarized light (π) at the transverse orientation of the magnetic field, the spectrum consists of eight lines which are grouped in two groups each of which consists of four lines. Each group has a special distinguished G-transition and the transition that is forbidden in the zero magnetic field. In the HPB regime, the probabilities of transitions in a group and derivatives of their frequency shifts with respect to the magnetic field asymptotically tend to magnitudes that are typical for the aforesaid distinguished G-transition. Some practical applications for the used microcell are mentioned.

DOI: 10.1134/S0030400X16120213

INTRODUCTION

The appearance of continuous-wave narrow-band (with a line width less than 1 MHz) diode lasers in the near-infrared range (700–900 nm) and strong permanent magnets have inspired renewed interest in studying the behavior of atomic levels of cesium, rubidium, and potassium in strong magnetic fields. Such investigations allow one to study in detail individual atomic transitions the behavior of which in a magnetic field turns out to be rather complex: probabilities of some atomic transitions decrease, while those of other transitions increase [1–3]. As a result, there remains only a strictly fixed number of atomic transitions. From the practical point of view, magnetooptical processes in vapors of Cs, Rb, and K atoms are successfully applied in narrow-band optical filters based on the Faraday effect [4] and in optical insulators [5], for the stabilization of the laser radiation frequency with respect to narrow atomic transitions shifted in strong magnetic fields [6], and in some other areas.

It is well known that, in strong magnetic fields, which are defined from the condition $B \gg B_0 = A_{\mathrm{HFS}}/\mu_B$, where A_{HFS} is the coupling coefficient of the hyperfine structure for the lower ground level and μ_B is the Bohr magneton (the constants were presented in [7]), total angular momentum of electrons **J** and nuclear spin **I** are decoupled. In this case, which is known as the hyperfine Paschen–Back (HPB) regime [8–11], the behavior of atomic levels is described better by projections m_J and m_I. The value B_0 for the potassium ^{39}K isotope is ~165 G, which is significantly less than the value B_0 for the cesium and rubidium isotopes ^{133}Cs (1.7 kG) and ^{87}Rb (2.4 kG). Due to smallness of the value B_0, the complete decoupling of **J** and **I** (i.e., the complete Paschen–Back regime) in ^{39}K occurs in relatively weak fields of ~1 kG. Since frequency intervals between transitions in such fields

(~100 MHz) are less than the Doppler width of an individual transition (900 MHz), applying Doppler-free spectroscopy is an important condition for successful observations of the HPB regime.

As shown in [12], using nanocells (NCs) with thicknesses $L = \lambda$ or $L = \lambda/2$, where $\lambda = 770$ nm is the wavelength of the resonance transition of the D_1-line of ^{39}K, allows one to successfully study the behavior of atomic transitions in a wide range of magnetic fields. An NC with thickness $L = \lambda = 770$ nm provides better spectral resolution, while an NC with thickness $L = \lambda/2 = 385$ nm provides better spatial resolution. The latter is important when using strongly inhomogeneous magnetic fields.

In spite of the undoubted advantages of NCs, they are yet not widespread due to complexity of manufacture [10]. This work is aimed at experimental demonstration of the fact that 10- to 30-μm-thick cells also can be successfully used for detailed investigations of atomic transitions of ^{39}K. In addition to the simplicity of manufacturing, it is important that the working temperature of a microcell (MC) with potassium (80–100°C) is significantly lower than the NC working temperature, reaching 150–180°C. As compared to ordinary cells with a centimeter length, the MC has the advantage that crossover resonances in saturated absorption (SA) spectra are suppressed [6]. From this point on, these resonances will be denoted as CO. The combination of qualities mentioned above allows one to successfully study atomic transitions in magnetic fields by use of SA spectra formed in an MC with potassium.

EXPERIMENT

A Spectroscopic Microcell with Potassium Vapors

MC windows with dimensions of 20 × 30 mm and a thickness of 2.3 mm were made of well-polished crystalline sapphire. To minimize birefringence, the windows were cut so that the **C** axis is perpendicular to their surface. To provide a gap with thickness $L \sim 30$ μm, thin platinum stripes were placed between inner surfaces of the windows. In the lower part of the windows, a hole was drilled into which a thin sapphire tube with a diameter of ~2 mm was inserted before gluing. The diameter of the inner hole of the tube was 0.8 mm. Molybdenum glass glued to the vacuum system was soldered to the sapphire tube. Then, filling with potassium is carried out in the same way as for glass cells. Details of the construction were presented in [13].

Let us compare MCs and NCs. First, manufacturing NCs is technically a more complicated problem due to the necessity to provide wide regions for which thicknesses of gaps between the inner surfaces are on the order of the wavelength and/or half-wavelength [10]. To form a gap in the case of MCs, it is sufficient to place thin platinum strips (spacers) with a necessary thickness (10–30 μm) between the inner surfaces of the windows. Since manufacturing of MCs also can cause definite technical difficulties, the proposed construction of a glass MC with sapphire windows was presented in Fig. 2 in [14]. Such an MC can be manufactured in many laboratories. Other constructions of MCs were presented in [15, 16].

Experimental Setup

Figure 1 presents the scheme of the experiment. The SA spectrum is recorded using an MC filled with potassium. The cell thickness in the direction of laser radiation propagation is 30 μm. The MC was placed into an oven with two holes for passing the laser radiation and heated to ~100°C, which provided an atomic density of $N \sim 2 \times 10^{11}$ cm^{-3}.

We used radiation of a tunable narrow-band extended cavity diode laser (ECDL) with a wavelength of 770 nm and width of ~1 MHz. The MC was placed between strong permanent magnets (PMs) with holes for the passage of laser radiation. The PMs were fixed on nonmagnetic tables. The magnetic field in the MC was varied by varying the distance between the PMs. Radiation with circular σ^+-polarization was formed using a $\lambda/4$ plate. A fraction of radiation passing through the MC was directed precisely backward using a mirror (M) (in this case, the incident radiation serves as pumping, while the reflected radiation serves as probe radiation) to form the SA spectrum in the MC. Neutral filters (not shown in the schematic) were used to select pumping and probe radiation optimum powers necessary for the formation of narrow atomic velocity selective optical pumping resonances (VSOPs) and reaching their relatively large amplitude at a small spectral width. To form the frequency reference, a fraction of the laser radiation was directed to an additional NC with thickness $L = \lambda$. In the transmission spectrum of this NS, VSOPs were formed at frequencies of atomic transitions $1, 2 \rightarrow 1', 2'$ (the primes mark upper levels) [17]. In some cases, the SA spectrum served as the frequency reference. For this purpose, a potassium cell with length $L = 1.4$ cm was used in node *4* and an SA scheme was assembled.

The insert in the upper left corner of Fig. 1 presents a diagram of four atomic transitions of the potassium ^{39}K isotope with indication of their relative probabilities. The orientation of the potassium MC with respect to wave vector $\mathbf{k}$ ($k = 2\pi/\lambda$) and strength vector of laser radiation electric field $\mathbf{E}$ is shown in the insert in the upper right corner of Fig. 1.

EXPERIMENTAL RESULTS AND DISCUSSION

The Case of σ^+-Polarized Laser Radiation

In Fig. 2a, the upper spectrum shows the saturated absorption spectrum in a cell with length $L = 1.4$ cm (the SA spectrum in a centimeter potassium cell was

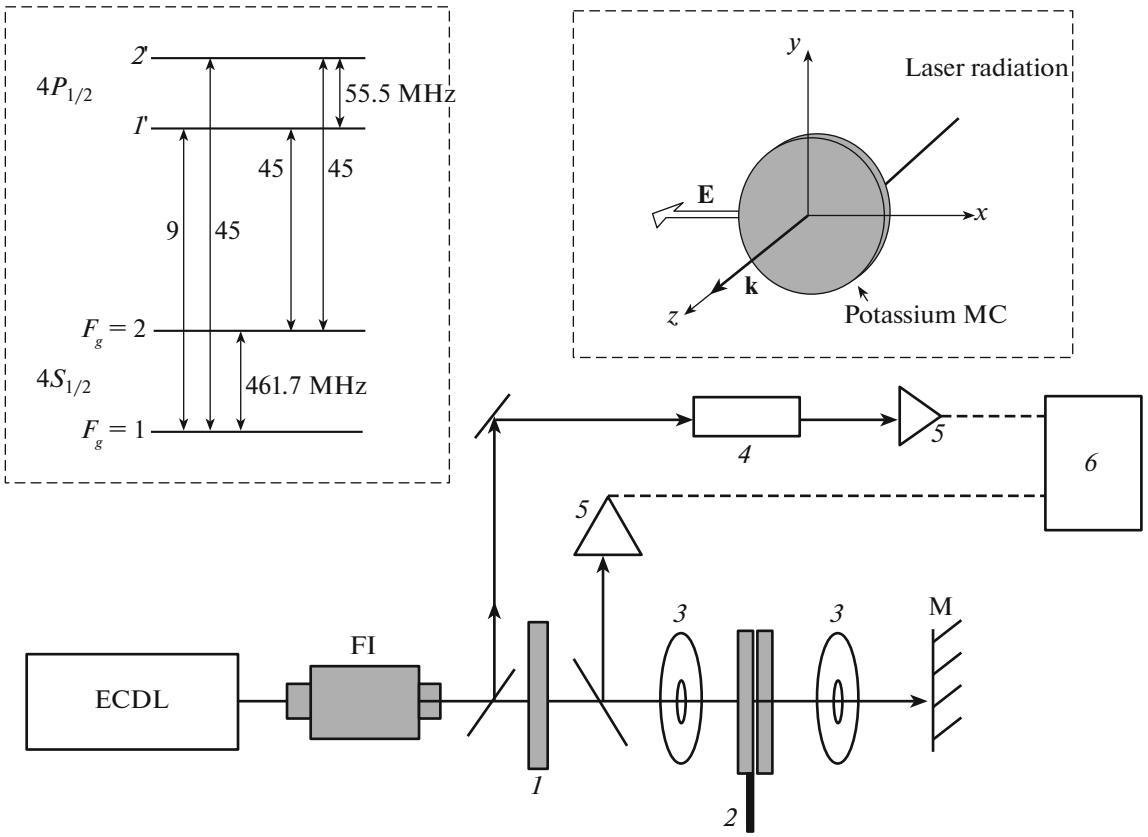

Fig. 1. Schematic of the experimental setup: (ECDL) diode laser, (FI) Faraday insulator, (*1*) quarter-wave plate, (*2*) microcell with potassium in the oven, (*3*) constant magnets with a hole for the laser beam, (*4*) node for the formation of the frequency reference system, (*5*) photoreceivers, (*6*) Tektronix TDS2014B four-ray digital oscilloscope, and (M) mirror.

also presented in [18]). It is seen that the spectrum contains five CO-resonances, together with narrow VSOPs positioned on atomic transitions 1, 2 → 1', 2'. Two of them (the largest ones) correspond to an increase in absorption. The lower curve shows the SA spectrum in an MC with length $L = 30$ μm. The CO-resonances are seen to be almost absent. Further decrease in thickness $L < 30$ μm allows one to completely suppress CO-resonances, but, at the same time, it becomes necessary to increase the temperature.

The possibility of suppressing crossover (CO) resonances in small thickness cells with the preservation of a good contrast of VSOPs is related to the fact that they are formed by atoms moving at different velocities. While VSOPs are formed by atoms that fly perpendicularly to pumping and probe field radiations, velocities of atoms making a contribution to crossover resonances have considerable projections onto the direction of laser beam propagation $v_z = 2\pi\varepsilon/k$, where ε is half of the frequency interval between the levels responsible for the formation of the crossover resonance. As was shown in [19], the time of flight of atoms with such velocities between cell windows L/v_z at $L \le 30$ μm is not sufficient to form a CO. At the same time, the atoms responsible for the formation of VSOPs have longitudinal velocities close to zero. Therefore, their time of interaction with the laser radiation is determined not by the longitudinal component of the velocity and distance between the cell windows, but by thermal velocity v_T and laser beam diameter $D = 3$ mm. This time, which is equal to D/v_T, turns out to be two orders of magnitude longer than in the case of crossover resonances and is quite sufficient to complete the process of optical pumping and formation of a VSOP.

In [20], weak magnetic fields were precisely measured using the SA spectrum in an ordinary cell with a length of 10 cm. However, even in fields with $B > 50$ G, the presence of a large number of split components of CO-resonances overlapping with each other and with the VSOP in the spectrum makes this method practically useless. As is shown below, CO-resonances are absent in MCs; for this reason, SA spectra remain a convenient tool for identifying atomic levels up to fields of several kilogauss.

Figure 2b shows SA spectra in longitudinal magnetic fields. In the spectra, one can see narrow VSOPs (~30 MHz) corresponding to reduced absorption. Magnetic field induction B increases upward and

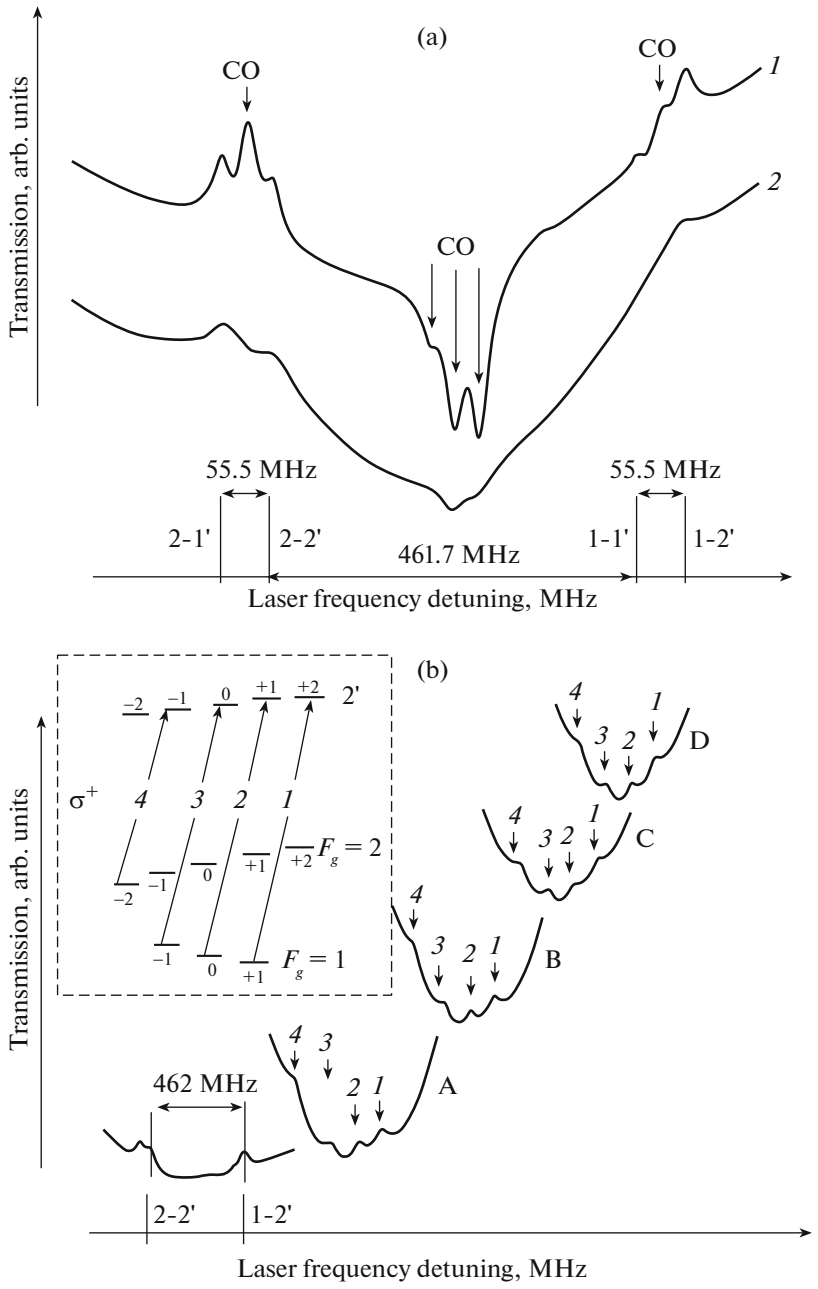

Fig. 2. (a) Upper curve *1* is the SA spectrum when using a potassium cell with length $L = 1.4$ cm. The spectrum contains four VSOPs and five CO-resonances. Lower curve *2* is the SA spectrum when using a potassium MC with length $L = 30$ μm. CO-resonances are almost absent. (b) Potassium MC with length $L = 30$ μm and σ^+-polarized radiation. SA spectra in magnetic fields for convenience, shifted along the vertical. Magnetic field induction B increases upward and amounts to 420, 720, 1000, and 1150 G for the spectra marked by letters A, B, C, and D, respectively. The lower curve is the reference spectrum. The insert shows the diagram of atomic levels and transitions between them (denoted by numbers *1–4*).

amounts to 420, 720, 1000, and 1150 G in the spectra marked by letters A, B, C, and D, respectively. The lower curve is the reference curve; it shows the frequency position of the transitions 1–2' and 2–2' (the frequency shifts of the atomic transitions were measured from the transition 2–2'). In the upper left corner, the atomic level and transitions denoted by the numbers 1–4 are shown. For atomic transitions between lower and upper levels, the selection rules $\Delta F = 0, \pm 1$ must be satisfied. In the case of σ^+-polarized radiation, the transitions occur between magnetic sublevels shown in the diagram according to the selection rules $\Delta m_F = m'_F - m_F = +1$. It is important to note that, in fields $B \gg B_0 = A_{\text{hfs}}/\mu_B \approx 165$ G, in contrast to weak magnetic fields, in which atomic level splitting is described by the total atomic moment $\mathbf{F} =$

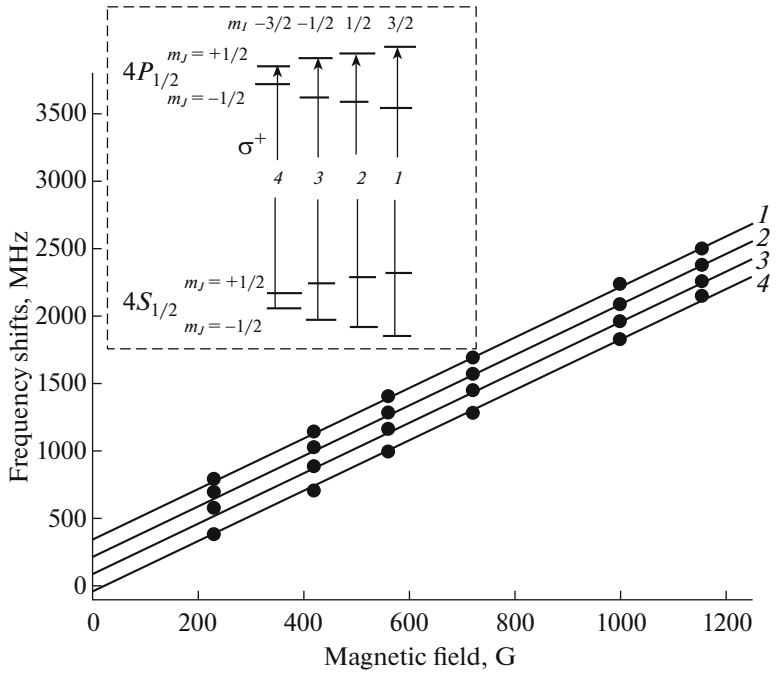

Fig. 3. The solid lines are the theoretical curves constructed by formula (1). The black circles are the experimental results. At $B >$ 600 G, the discrepancy between the experiment and theory is less than 2%. The insert shows atomic transitions in the basis of projections m_J and m_I.

J + **I** and its projection m_F, where **J** is the total angular momentum of the electron shell of atom and **I** is the nuclear spin (for the potassium ^{39}K isotope, $I = 3/2$), decoupling between **J** and **I** begins. In strong magnetic fields, atomic level splitting is described by projections m_J and m_I (see the insert in Fig. 3) [8–12]. This results in the fact that the number of detected atomic transitions for ^{39}K is reduced from 12 to 4 (probabilities of other eight transitions in fields larger than 100 G tend to zero). The number of transitions (four) does not change with the further increase in the magnetic field. In the HPB regime, derivatives of frequency shifts with respect to the magnetic field s (MHz/G) and probabilities of atomic transitions in one group are determined by fixed values of projections m_J of the lower and upper levels and tend to the same value within the group. It is seen from the spectra presented in Fig. 2b that the amplitudes of transitions 1–4 are approximately equal and the frequency intervals are also approximately the same. It is important to note that the frequency position of transitions, frequency distance between them, and frequency slopes of s for the D_1-line in the HPB regime are determined from a simple analytical expression [21]:

$$E_{|J,m_J,I,m_I\rangle} = A_{\mathrm{HFS}} m_J m_I + \mu_B (g_J m_J + g_I m_I) B, \quad (1)$$

where the Landé factors for total electron momentum g_J and nuclear momentum g_I for ^{39}K were presented in [7]. Note that coupling coefficient of the hyperfine structure $A_{\mathrm{HFS}}(S)$ for $4S_{1/2}$ is half the hyperfine splitting of the lower level (0.5 × 462 MHz) and coupling coefficient $A_{\mathrm{HFS}}(P)$ for $4P_{1/2}$ is half the hyperfine splitting of the upper level (0.5 × 55.5 MHz). In the HPB regime, it follows from Eq. (1) that the frequency interval between neighboring transitions 1, 2, 3, and 4 is determined as $0.5[A_{\mathrm{HFS}}(S) + A_{\mathrm{HFS}}(P)] \approx 130$ MHz, which is verified experimentally. By a similar simple expression, one can determine the frequency distance between two neighboring transitions of the D_1-lines of ^{87}Rb, Na, ^{41}K, etc. Since the Doppler width for ^{39}K vapors is ~900 MHz (at a temperature of ~100°C), using an ordinary millimeter or centimeter potassium cell for spectral resolution of transitions 1, 2, 3, and 4 is useless. In Fig. 3, the solid lines were constructed by formula (1) and the black circles are the experimental results. It is seen that a good agreement begins to be observed at $B \geq 4B_0$. The insert in Fig. 3 shows transitions in the basis of projections m_J and m_I with selection rules $\Delta m_J = m_J' - m_J = +1$ and $\Delta m_I = m_I' - m_I = 0$ for σ+-radiation.

The Case of π-Polarized Laser Radiation

In this case, the quarter-plate is removed and radiation is linearly polarized. The permanent magnets are placed so that magnetic field **B** is directed along the vector of laser field strength **E** (see the insert in Fig. 1) [22]. In this case, the atomic transitions shown in Fig. 4 take place.

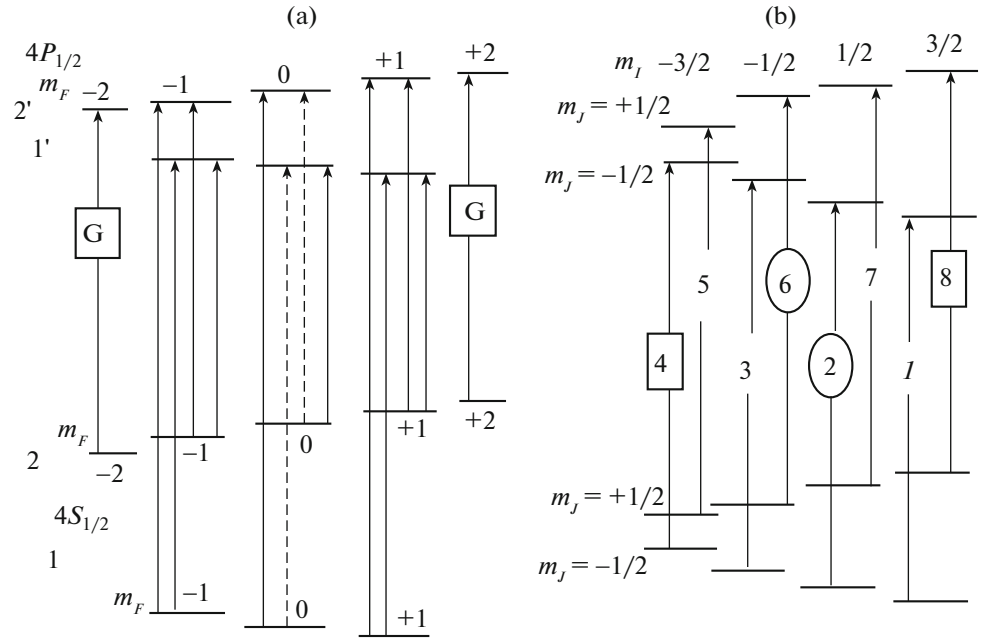

Fig. 4. (a) Diagram of atomic transitions of the D_1-line of ^{39}K (14 components) in magnetic field $B < B_0$ in the case of π-polarized radiation ($\Delta F = 0, \pm 1$, $\Delta m_F = 0$, the dashed transitions are forbidden). The squares mark G-transitions. (b) Diagram of atomic transitions of the D_1-line of ^{39}K (eight components) in magnetic field $B \gg B_0$ (the HPB regime) in the case of π-polarized radiation ($\Delta m_J = 0$ and $\Delta m_I = 0$). The squares mark G-transitions; the ovals, FZF-transitions.

It is well known that, in strong magnetic fields, the probabilities of optical range atomic transitions beginning and ending at different magnetic sublevels m_F of the lower and upper levels considerably vary [1, 2]. To do this, it is sufficient that the perturbation induced by the external magnetic field causes an "intermixing" of at least one sublevel m_F of the lower or upper level F with a magnetic sublevel of other level $F \pm 1$ at constant values of quantum numbers L, J, and m_F [1–3, 12]. As is seen from Fig. 4a, for two lateral ^{39}K transitions ($F = 2$, $m_F = \pm 2 \rightarrow F' = 2$, $m'_F = \pm 2$) marked in the figures by the letter G, there are no neighboring magnetic sublevels with which intermixing can occur, both for lower magnetic sublevel m_F and for upper one m'_F; the probabilities of these transitions do not depend on the magnetic field. Probabilities of other transitions are subjected to modifications. In [23], these transitions were called "guiding atomic transitions" and denoted by the letter G. In the same work, it was shown that G-transitions are present in all systems of D_1-lines of alkali metal atoms in the case of linear (π) polarization; for D_2-lines, there are no G-transitions [22]. The probabilities of all atomic transitions in each group, as well as derivatives s of their frequency shifts with respect to the magnetic field in strong transverse magnetic fields, asymptotically tend to values inherent to G-transitions (see the insert in Fig. 5). We again note that probabilities and derivatives s of their frequency shifts with respect to the magnetic field for G-transitions do not depend on the magnitude of the magnetic field and remain the same as they were in the zero magnetic field. Since such constants in the zero magnetic field are presented in reference books [7, 21], they can be predicted also for other atomic transitions in their group in the HPB regime (see the insert in Fig. 5). In the diagram of Fig. 4a, there are two more interesting atomic transitions denoted by dashed lines. Since these transitions are forbidden in a zero magnetic field according to the selection rules $\Delta F = 0, \pm 1$, $\Delta m_F = 0$, they are denoted by letters FZF. However, in strong magnetic fields, the probabilities of FZF-transitions rapidly grow and asymptotically tend to values inherent to G-transitions. The diagram in Fig. 4b shows eight atomic transitions in the basis of projections m_J and m_I with the selection rules $\Delta m_J = m'_J - m_J = 0$ and $\Delta m_I = m'_I - m_I = 0$ for π-radiation. Therefore, the number of atomic transitions at $B \gg B_0$ is reduced from the initial 14 (Fig. 4a) to 8. The last number remains unchanged with further increase in the magnetic field. The probability of another six atomic transitions in fields exceeding 100 G rapidly decreases to zero [12]. The eight transitions are divided into two groups. This behavior of atomic transitions is also typical for the HPB regime.

Figure 5 (upper curve) presents the SA for π-polarized radiation, laser power of 0.3 mW, MC temperature of 110°C, and transverse magnetic field of 520 G. Transitions nos. 4 and 8 (G-transitions) are marked by rectangles; transitions nos. 2 and 6 (FZF-transitions),

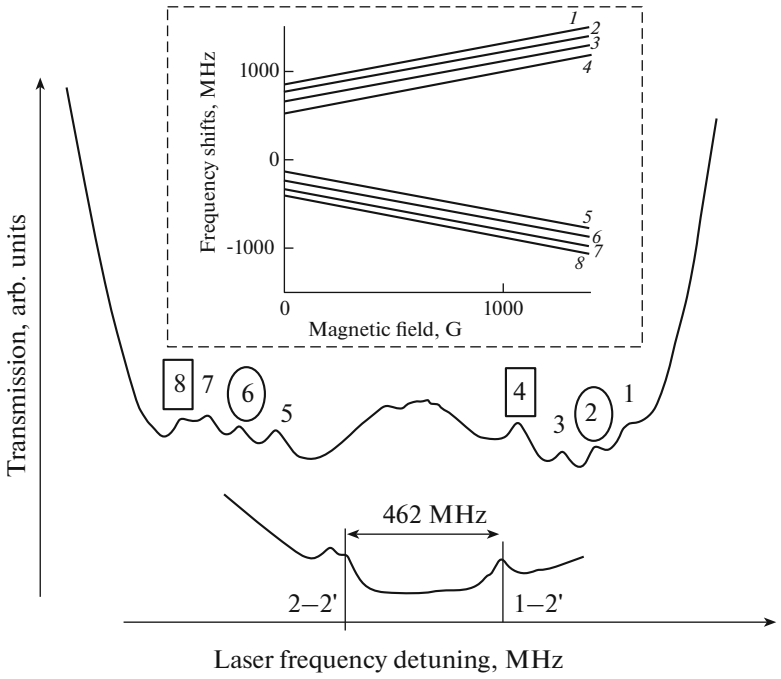

Fig. 5. ^{39}K, π-polarized radiation. The upper curve corresponds to the SA spectrum, transverse magnetic field, $B = 520$ G, eight atomic transitions manifest themselves in the form of eight VSOPs. Transitions nos. *4* and *8* (G-transitions) are marked by rectangles; transitions nos. *2* and *6*, (FZF-transitions), by ovals. The lower curve is the reference curve. The insert shows two separate groups, with four transitions in each group: transitions *1–4* and *5–8*; curves *1–8* were constructed by formula (1).

by ovals. It is seen that all the eight transitions are well resolved, which agrees with the statement that probabilities of transitions in each group (including the FZF-transitions) in the HPB regime asymptotically tend to values inherent to G-transitions. The insert in Fig. 5 shows two separate groups, with four transitions in each group. Curves *1–8* were constructed by formula (1), which is valid for the HPB regime. Note that the presence of two groups with four transitions in each group agrees with the diagram presented in Fig. 4b. The frequency slopes of four transitions in each group are specified by transitions nos. 4 and 8 (G-transitions). Note that the agreement of the experiment with theoretical curves when using an MC is as good (error of less than 2%) as was observed when using an NC in [12].

The HPB regime on potassium vapors was recently studied using the process of electromagnetically induced transparency (EIT) [24] from the specific behavior of the group of EIT-resonances. However, since EIT-resonances disappeared at $B > 100$ G, only the beginning of the HPB regime was detected, because observing the total regime needs fields with $B \gg 160$ G. This was successfully implemented in this work.

CONCLUSIONS

In this work, it has been shown that crossover resonances are almost absent in the SA spectrum in an MC having thickness $L = 30$ μm and filled with potassium vapors. In addition, the spectral width of VSOPs formed in it is small (~30 MHz). This allows one to use the SA spectrum for studying the frequency position and probabilities of individual atomic transitions in strong magnetic fields. Since the potassium ^{39}K isotope has the smallest value $A_{hfs}/\mu_B \approx 165$ G of all alkali metals, this allowed us to observe the decoupling between **J** and **I** (the HPB regime) in moderate magnetic fields $B > 500$ G.

In the case of using σ^+-polarized radiation in the HPB regime, four almost equidistantly positioned atomic transitions with almost equal amplitudes are detected. The dependence of the frequency position of atomic transitions on magnetic field induction B is well described by formula (1).

In the case of using the π-polarized laser radiation and transverse magnetic field in the HPB regime, the spectrum consists of eight atomic transitions which are regrouped in two groups separated with respect to frequency by four transitions in each group. Each group contains a special directing G-transition and FZF-transition, i.e., a transition forbidden for a zero magnetic field. In the HPB regime, probabilities of transitions in a group (including the FZF-transition) and their frequency slopes asymptotically tend to the same value typical for the G-transition. Since the frequency intervals between transitions are on the order of 100 MHz, they should be studied by spectroscopy

free from the Doppler broadening, which is provided by the SA technique with the use of MCs.

Note that all the above-mentioned features of the HPB regime for ^{39}K will be also observed for ^{87}Rb, which has a similar structure of transitions. However, due to large frequency splittings of the hyperfine structure and, as a consequence, large value of B_0, the magnetic fields required for ^{87}Rb are approximately 15 times stronger [11].

Let us single out the following practical applications of MCs: (i) formation of the frequency reference at strongly shifted (with respect to initial atomic levels of ^{39}K) frequencies of up to $\pm$4 GHz, (ii) referencing of the laser frequency (stabilization) to shifted atomic levels [8], and (iii) mapping of strongly inhomogeneous magnetic fields with 30-μm spatial resolution.

The simple setup described in this work and consisting of a thin potassium cell, available diode laser, and permanent magnet can serve as the basis of a vivid demonstrational laboratory work for students on observing features of decoupling between angular momentums of the electron and nuclear subsystems of the atom.

ACKNOWLEDGMENTS

We are grateful to A.S. Sarkisyan for preparing the MCs.

The investigation was carried out in the scope of a joint Armenian–Russian scientific project and supported by the State Committee of Science of the Republic of Armenia (project no. 15RF-024) and Russian Foundation for Basic Research (project no. 15-52-05030). T.A. Vartanyan participates in State Project no. 2014/190.

REFERENCES

1. E. B. Aleksandrov, G. I. Khvostenko, and M. P. Chaika, *Interference of Atomic States* (Nauka, Moscow, 1991) [in Russian].
2. A. Sargsyan, A. Tonoyan, G. Hakhumyan, et al., Laser Phys. Lett. **11**, 055701 (2014).
3. G. Hakhumyan, C. Leroy, R. Mirzoyan, Y. Pashayan-Leroy, and D. Sarkisyan, Eur. Phys. J. D **66**, 119 (2012).
4. M. A. Zentile, D. J. Whiting, J. Keaveney, et al., Opt. Lett. **40**, 2000 (2015).
5. M. A. Zentile, R. Andrews, L. Weller, et al., J. Phys. B: At., Mol., Opt. Phys. **47**, 075005 (2014).
6. A. Sargsyan, A. Tonoyan, R. Mirzoyan, D. Sarkisyan, A. Wojciechowski, A. Stabrawa, and W. Gawlik, Opt. Lett. **39**, 2270 (2014).
7. M. A. Zentile, J. S. Keaveney, L. Weller, et al., Comput. Phys. Commun. **189**, 162 (2015).
8. B. A. Olsen, B. Patton, Y.-Y. Jau, et al., Phys. Rev. A **84**, 063410 (2011).
9. A. Sargsyan, G. Hakhumyan, C. Leroy, et al., Opt. Lett. **37**, 1379 (2012).
10. A. Sargsyan, G. Hakhumyan, R. Mirzoyan, and D. Sarkisyan, JETP Lett. **98**, 441 (2013).
11. A. Sargsyan, G. Hakhumyan, C. Leroy, Y. Pashayan-Leroy, A. Papoyan, D. Sarkisyan, and M. Auzinsh, J. Opt. Soc. Am. B **31**, 1046 (2014).
12. A. Sargsyan, A. Tonoyan, G. Hakhumyan, C. Leroy, Y. Pashayan-Leroy, and D. Sarkisyan, Europhys. Lett. **110**, 23001 (2015).
13. A. Sargsyan, M. G. Bason, D. Sarkisyan, A. K. Mohapatra, and C. S. Adams, Opt. Spectrosc. **109**, 529 (2010).
14. A. Sargsyan, B. Glushko, and D. Sarkisyan, J. Exp. Theor. Phys. **120**, 579 (2015).
15. T. Baluktsian, C. Urban, T. Bublat, H. Giessen, R. Löw, and T. Pfau, Opt. Lett. **35**, 1950 (2010).
16. K. A. Whittaker, J. Keaveney, I. G. Hughes, A. Sargsyan, D. Sarkisyan, B. Gmeiner, V. Sandoghdar, and C. S. Adams, J. Phys.: Conf. Ser. **635**, 122006 (2015).
17. A. Sargsyan, G. Hakhumyan, A. Papoyan, et al., Appl. Phys. Lett. **93**, 021119 (2008).
18. D. Bloch, M. Ducloy, et al., Laser Phys. **6**, 670 (1996).
19. A. Sargsyan, D. Sarkisyan, A. Papoyan, et al., Laser Phys. **18**, 749 (2008).
20. J. A. Zieliska, F. A. Beduini, N. Godbout, and M. W. Mitchell, Opt. Lett. **37**, 524 (2012).
21. D. A. Steck, Rubidium 87 d line data. http://steck.us/alkalidata.
22. A. Sargsyan, G. Hakhumyan, A. Tonoyan, P. A. Petrov, and T. A. Vartanyan, Opt. Spectrosc. **119**, 202 (2015).
23. A. Sargsyan, G. Hakhumyan, A. Papoyan, and D. Sarkisyan, JETP Lett. **101**, 303 (2015).
24. A. Sargsyan, P. A. Petrov, T. A. Vartanyan, and D. Sarkisyan, Opt. Spectrosc. **120**, 339 (2016).

Translated by A. Nikol'skii